Hindawi Publishing Corporation
Advances in Materials Science and Engineering
Volume 2015, Article ID 670243, 10 pages
http://dx.doi.org/10.1155/2015/670243

Research Article

First-Principles Study on the Structural and Electronic Properties of N Atoms Doped-Rutile TiO_2 of Oxygen Vacancies

Zhong-Liang Zeng

College of Earth Sciences, China University of Geosciences, Wuhan 430074, China

Correspondence should be addressed to Zhong-Liang Zeng; dillon117@163.com

Received 18 March 2014; Revised 19 July 2014; Accepted 22 July 2014

Academic Editor: Guocheng Lv

For the propose of considering the actual situation of electronic neutral, a simulation has been down on the basis of choosing the position of dual N and researching the oxygen vacancy. It is found that the reason why crystal material gets smaller is due to the emergence of impurity levels. By introducing the oxygen vacancy to the structure, the results show that while the oxygen vacancy is near the two nitrogen atoms which have a back to back position, its energy gets the lowest level and its structure gets the most stable state. From its energy band structure and density, the author finds that the impurity elements do not affect the migration of Fermi level while the oxygen vacancy has been increased. Instead of that, the conduction band of metal atoms moves to the Fermi level and then forms the N-type semiconductor material, but the photocatalytic activity is not as good as the dual N-doping state.

1. Introduction

Since the discovery of TiO_2 Fujisima-Honda [1] effect exists, different preparation methods have been used to further enhance the photocatalytic performance of TiO_2. N doped TiO_2 catalyst which is used for improving the ability of visible light shows good effect [2–10]. But in the TiO_2 photocatalytic material preparation process, the oxygen vacancy is an intrinsic defect, that is very easy to occur [11], though researchers have done a lot of research on it [12–21], However, the different methods of calculation results are not totally unanimous.

Research shows that the most common form of a defect of three-dimensional periodic crystals is vacancy defects, which will affect the physical properties of the material, and the oxygen vacancies are also more prone to N doped TiO_2 system [22–24]. However, effect of oxygen vacancy on the electronic structure and optical activity is still not very clear. On one hand, the oxygen vacancy is the key factor causing visible light photocatalytic activity [25–29]. But it is discussed by Irie et al. [30] that, with increasing N content, the amounts of oxygen vacancies act as recombination centers electron hole, which reduces the visible light photocatalytic activity. It is N doped TiO_2 with oxygen vacancies which is studied through theoretical and experimental methods by Wang et al. [31]. They believe that the doping of N and Vo both can cause the red shift of absorption edge to visible light region. However, as oxygen vacancies and Ti^{3+} act as a recombination center electron hole, it is not conducive to visible light photocatalytic activity increase. So the electronic structure of point defects in the study that will be important for understanding the characteristics of TiO_2 materials plays a role.

Although the photocatalytic effect of single rutile is not as good as anatase [32], in fact, rutile TiO_2 also has higher photocatalytic activity in the degradation of some pollutants; under certain conditions, rutile and anatase particles can be synergistic [33–35]. Therefore, research on doped rutile has some practical needs.

Based on the density functional theory (DFT), the plane-wave ultrasoft pseudopotential method has been successfully applied to study the electronic structure and dynamical properties for variety of materials [36–42] in order to more clearly reveal the influence of N element and oxygen vacancies of rutile geometry and electronic structure. Based on the first-principles density functional theory of energy band calculation method and the super cell model, this paper has taken a geometrical optimization for the rutile-TiO_2

Table 1: Comparisons of lattice constants between calculation (including those obtained in another work) and experiment.

	Exp. [47]	This work	Relative error	Another work [45]
a/nm	0.45929 ± 0.00005	0.4594	2.3950×10^{-2}%	0.4594
c/nm	0.29591 ± 0.00003	0.2959	3.3794×10^{-3}%	0.2959
U	0.03056 ± 0.00006	0.03059	9.8168×10^{-2}%	0.03059

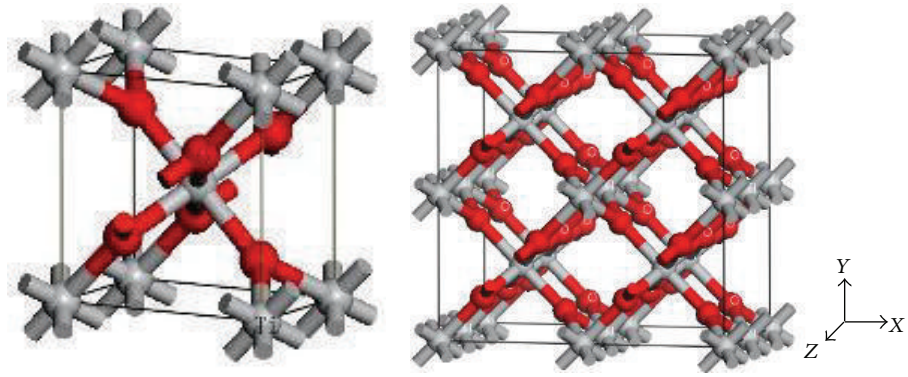

(a) (b)

Figure 1: (a) The structure of rutile TiO_2 primitive cell. (b) The super cell structure of rutile TiO_2 $(2 \times 2 \times 2)$.

doped N elements and analyzes the geometric structure and electronic structure of the double nitrogen. After that, the paper theoretically analyzes the oxygen vacancy doping cases and its related properties.

2. The Computational Model and Method

Rutile TiO_2 has a tetragonal crystal structure, with a space group of P42/MNM. In this paper, we employed the rutile-phase TiO_2 single cell and super cell $(2 \times 2 \times 2)$ models as shown in Figures 1(a) and 1(b). The super cell model consists of eight single cells, which were arrayed along the x-axis, y-axis, and z-axis. The crystal structure formula is $Ti_{16}O_{32}$.

The calculation in this paper is based on the wavelet plane ultrasoft pseudopotential method. In order to minimize the number of plane waves, we apply ultrasoft pseudopotential to describe the ion-core interaction with the valence electrons. In the reciprocal k-space, the cut-off energy is selected as 300 eV, the generalized gradient approximation (GGA) [43] method is used in the work. The integral calculation of total system energy and charge density which works in the Brillouin zone takes the Monkhorst-Pack scheme to select the k grid as $2 \times 2 \times 7$. In the calculation, the involved valence electron configurations are O $2s^2 2p^4$, N $2s^2 2p^3$, and Ti $3s^2 3p^6 3d^2 4s$. The calculation is accomplished by employing CASTEP [44] quantum mechanics module which is based on density functional theory, and the software package is MS4.4 version.

3. The Calculation Results

3.1. Pure Rutile Lattice Constant and Electronic Structure. Firstly, we carry out structural optimization of TiO_2 and then we obtain the rutile phase TiO_2 lattice constants and energy band structures. The lattice constant parameters are listed in Table 1, and the experimental data are also included in the table. Apparently, Our calculation results are well consistent with the experimental and the predecessors' simulated results.

The rutile TiO_2 band structure and density of states are shown in Figure 2, the Fermi level has been chosen at zero-point energy, which is shown as dotted line in the figure. The calculated band gap is 2.048 eV, which is less than the experimental value of 3.0 eV, while it matches the band gap of 1.9 eV calculated by Song et al. [45]. As we all know that a certain degree of bias by DFT [45, 46] in the calculation of electronic band structure.

Based on the above calculation of pure rutile, we can determine that the method of calculation is suitable for doped TiO_2 System.

For comparison, we also optimized a single N atom doped-rutile structure; then we obtained its geometric structure and electronic properties. Figure 3 shows the models of geometry diagram about a N atom and two-N-atom doped TiO_2 on different positions. By optimizing the geometries, then we calculated the total energy, energy band gap, and the distances between the two impurity N atoms; the related parameters are listed in Table 2.

For the two-N-atom doped TiO_2, for convenience, in this paper, we take a Ti atom as the benchmark calibration; in the three models of two-N-atom doped structure, the N atoms in the same position are labeled N1, N atoms changes in position are written as N2. Through geometry optimization, it can be found that when the two doped N atoms have a minimum distance (the minimum is 0.2546 nm), the structure has the lowest energy, with the highest stability. This indicates that if N atoms doped in rutile TiO_2, it will take the nearest neighbor

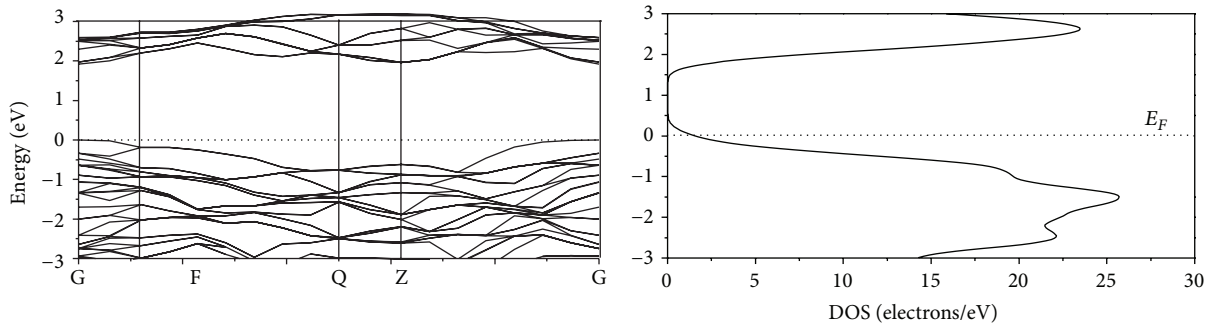

FIGURE 2: (a) The band structure of rutile TiO_2. (b) The total density of rutile TiO_2.

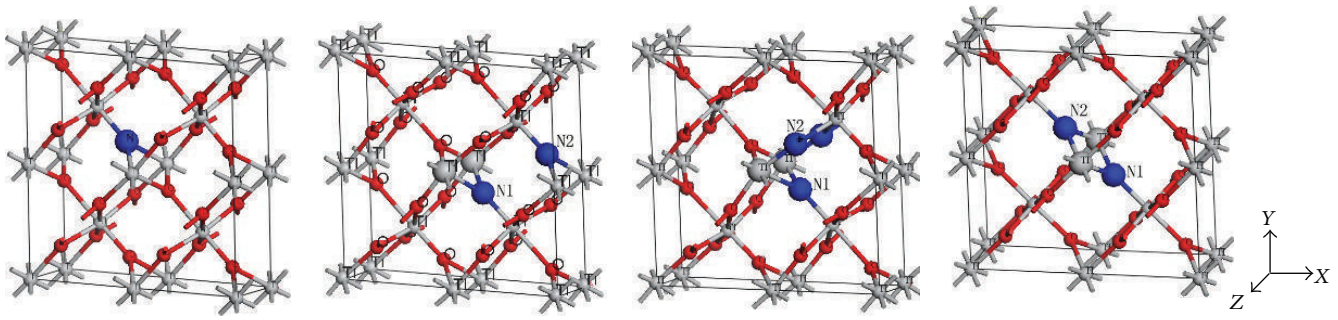

FIGURE 3: The structures of single N doped and double N doped-rutile TiO_2. (a) Single N doped TiO_2: (b) Model A of double N doped-TiO_2; (c) Model B of double N doped TiO_2; (d) Model C of double N doped-TiO_2.

occupancy mode. By comparing Figures 3(b), 3(c), 3(d), and 1(b) we find that doping will result in different levels of local deformation. Comparing the data in Table 2, it seems that when the location of N atoms is in the adjacent position, the two doped N atoms will affect one another.

Considering N atom has one electron less than O atom, the two N atoms in the adjacent position can share electrons more easily and then reach a steady state; from the optimized model in Figure 3(b), we also found that if two N atoms are close to each other, the N–N bond has the shortest distance; the structural optimization parameters are consistent with the above analysis.

3.2. Comparative Analysis of Six Kinds of $Ti_{16}O_{30}N_2$ Model. When creating a dual N super cell $Ti_{16}O_{32}$ for orthodoping, taking into account the bond lengths, bond angles, and symmetry, it is still possible to build six different types of doping methods. This paper considers mainly six kinds of geometrical and electronic structure analysis.

3.2.1. The Geometrical Structure of the Six Models of $Ti_{16}O_{30}N_2$. Figure 4 is a pair of N-atom super cells in $Ti_{16}O_{32}$ oxygen doping orthosubstitution optimized geometric structure. By optimizing calculation, the total energy, energy band gap, and the distance between the two impurity atoms have been listed in Table 3. After the geometry optimization, by Energy band analyzing and the size of the bond angle between N–O–N and the atomic distance of N–N, we identified six calibration models which are named Model 1 ($Ti_{16}O_{30}N_2$_1), Model 2 ($Ti_{16}O_{30}N_2$_2), Model 3 ($Ti_{16}O_{30}N_2$_3), Model 4 ($Ti_{16}O_{30}N_2$_4), Model 5 ($Ti_{16}O_{30}N_2$_5), and Model 6 ($Ti_{16}O_{30}N_2$_6).

The results show that the pure direct band gap of $Ti_{16}O_{32}$ is 1.887 ev which is different from the band gap Ti_8O_{16} (1.921 ev). As we get the result under a professional analysis, the calculation is precise. Therefore, it must comply with the same initial conditions and computing platform when we make a horizontal contrast. For the same object we can exclude the difference caused by different software versions. Qualitative analysis has been used to analyze the property of the six different models. After having a geometry optimization, the distance between the two nitrogen atoms gets its minimum. When the minimum gets 0.1372 mm, the smallest band gap becomes 1.498 ev. It indicates that while the N atom doped into rutile, it will occupy the nearest neighbor position. By comparing Figures 4(a), 4(b), 4(c), 4(d), and 4(f) with Figure 1, we find there is a replacement bit with different degree of local deformation replacement. With the data in Table 3, take into account that O atoms lack one electron than N atoms, while two N atoms that are in adjacent positions can be better sharing electrons and it is easier to achieve steady state. From Table 3 we also found $Ti_{16}O_{30}N_2$_1 minimum total energy model, and it is also more stable. Combining with

Table 2: The total energy and band gaps of rutile and four kinds of N-doped rutile TiO_2 and the bond distance between the two doped N–N.

	Final free energy (eV)	Energy gaps (eV)	Atomic distance of N–N (nm)
Ti_8O_{16}	−19890.0596	2.048	—
$Ti_8O_{15}N$	−19678.9163	1.553	—
Model A	−19552.3673	1.63	0.3377
Model B	−19552.8169	1.24	0.2546
Model C	−19552.2915	1.28	0.2715

Table 3: The total energy and band gaps of rutile and six kinds of N-doped rutile TiO_2 and the bond distance between the two doped N–N and Angle of N–Ti–N.

	Final free energy (eV)	Energy gap (eV)	Atomic distance of N–N (nm)	Angle of N–Ti–N
$Ti_{16}O_{32}$	−39780.209	1.887	0.2780 (O–O)	90.000 (O–Ti–O)
$Ti_{16}O_{30}N_2$_1	−39444.4974	1.508	0.1373	39.968
$Ti_{16}O_{30}N_2$_2	−39444.4952	1.501	0.1373	39.924
$Ti_{16}O_{30}N_2$_3	−39444.4928	1.498	0.1372	39.975
$Ti_{16}O_{30}N_2$_4	−39444.4949	1.502	0.1372	39.914
$Ti_{16}O_{30}N_2$_5	−39442.4369	0.182	0.2602	84.036
$Ti_{16}O_{30}N_2$_6	−39442.4177	0.208	0.2959	95.114

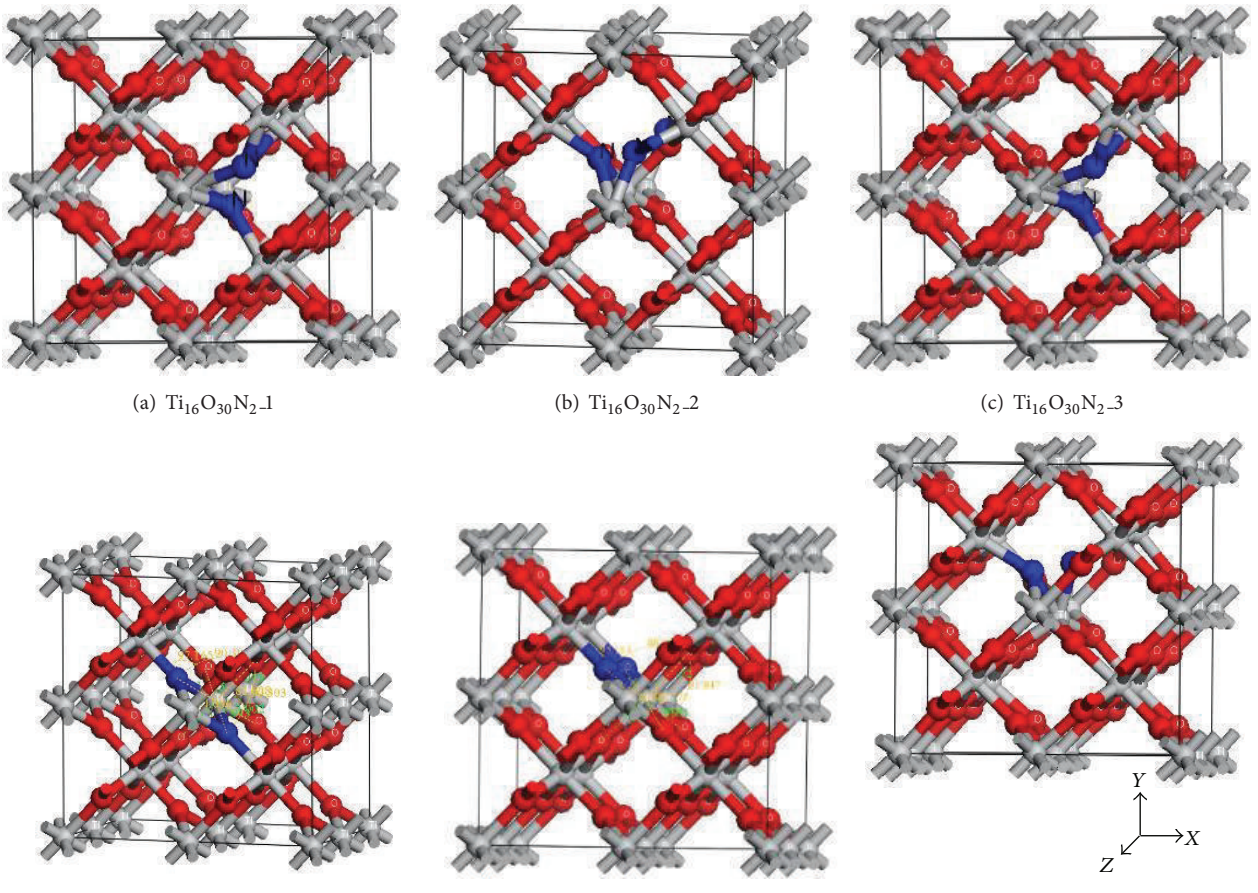

(a) $Ti_{16}O_{30}N_2$_1 (b) $Ti_{16}O_{30}N_2$_2 (c) $Ti_{16}O_{30}N_2$_3

(d) $Ti_{16}O_{30}N_2$_4 (e) $Ti_{16}O_{30}N_2$_5 (f) $Ti_{16}O_{30}N_2$_6

Figure 4: The structures of six kinds of $Ti_{16}O_{30}N_2$.

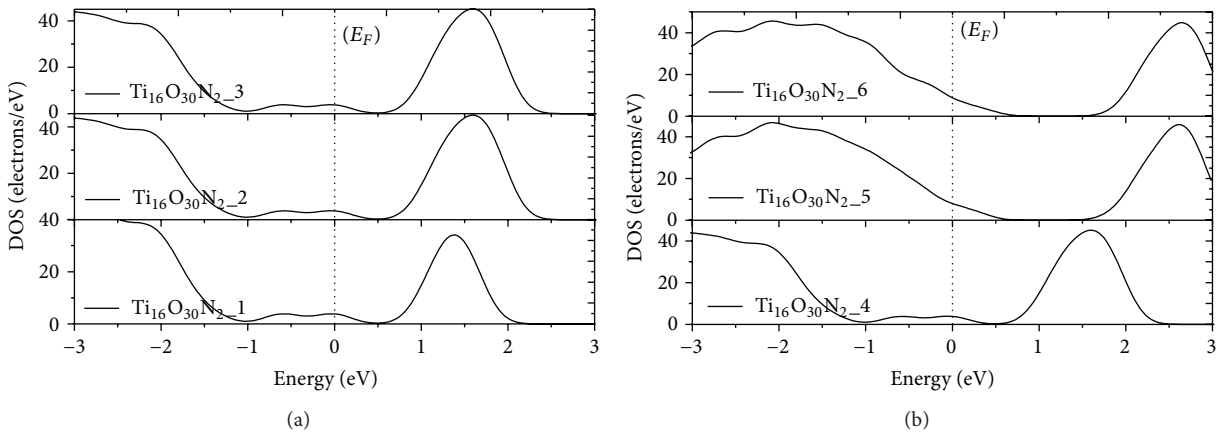

Figure 5: The total density of states of six kinds of $Ti_{16}O_{30}N_2$ model.

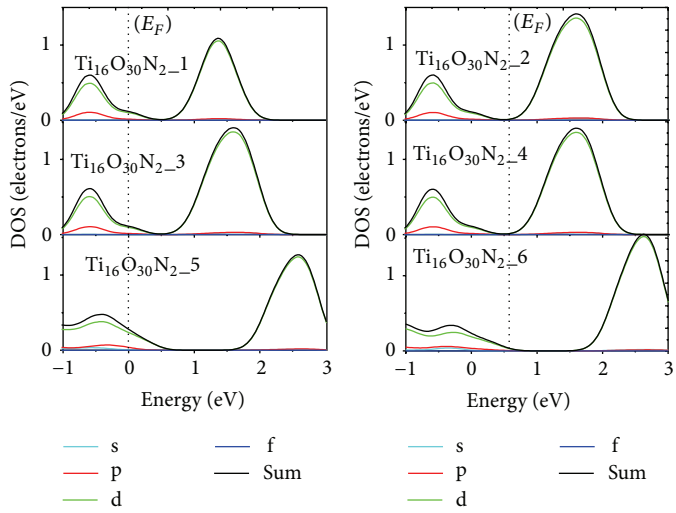

Figure 6: The density of states of Ti atom.

the author's dual N doped in the conclusions of the study, he finds that $Ti_{16}O_{30}N_2\_1$ may be more closer to the actual state.

3.2.2. The Electronic Structure of Six Kinds of $Ti_{16}O_{30}N_2$ Model. Figure 5 shows the density graph of six models. From Figures 5 and 4(a) we find that the band gap of TiO_2 has been changed. The calculated band gap has been shown in Table 3. The generated doping which occurred during O atoms replaced N atoms has been apparently reduced. However, it shows band gap minimum in Model 5 and Model 6 which is much lower than the normal band gap. It is due to the Fermi level caused through the band. From the energy band structure of the state we saw that a small amount of energy level cross the Fermi energy level, since the band gap cannot be accurately obtained.

From Figure 5 we can see the density graph of Model 5 and Model 6 is different from the other four models. It is mainly reflected by smaller direct band gap, which is farther from band Fermi level. The valence band is closer to Fermi level which is only 0.208 ev. This is because the Fermi level has crossed the band level, so the material gets metallic character. We can no longer classify it as a semiconductor material and the band gap cannot be given directly.

Figures 6 and 7 show us the density graph of N-atom and Ti atom. From Figure 7, we see N 2p orbital located in the middle band, which forms an intermediate level. It indicates that the introduction of N atom will better change the band gap. Since the density near the Fermi energy of Model 1, Model 2, Model 3, and Model 4 is low, and the band gap is small there, thus they will more likely result in excitation phenomenon. The density of N atoms of Models 5 and 6 near the Fermi energy is very large, but its band gap is wide. With Figures 5, 6, and 7 we can conclude that the dope of the first four models may affect the valence of Ti atom. The valence band energy level may have a certain extension to higher level, but there are not any prominent changes in conduction band. Besides, the width and lower restrict of the guiding band do not change significantly, while near the Fermi level it showed a more gentle impurity energy level. For Models 5 and 6, their conduction band has been removed away from Fermi level. According to the contents in Table 3, we found that when

Table 4: The total energy and band gaps of rutile and eight kinds of neutral doped rutile TiO_2 and the bond distance between the two doped N–N and angle of N–Ti–N.

	Final free energy (eV)	Energy gap (eV)	Atomic distance of N–N (nm)	Angle of N–Ti–N
$Ti_{16}O_{29}N_2$_1	−39003.2719	—	0.1369	39.934
$Ti_{16}O_{29}N_2$_2	−39004.1026	0.014	0.1373	39.968
$Ti_{16}O_{29}N_2$_3	−39003.568	—	0.1388	40.475
$Ti_{16}O_{29}N_2$_4	−39003.7126	—	0.1372	39.914
$Ti_{16}O_{29}N_2$_5	−39003.5715	0.008	0.1373	39.968
$Ti_{16}O_{29}N_2$_6	−39003.7321	0.040	0.1371	40.104
$Ti_{16}O_{29}N_2$_7	−39004.4015	—	0.1420	42.348
$Ti_{16}O_{29}N_2$_8	−39004.1177	0.014	0.1367	38.307

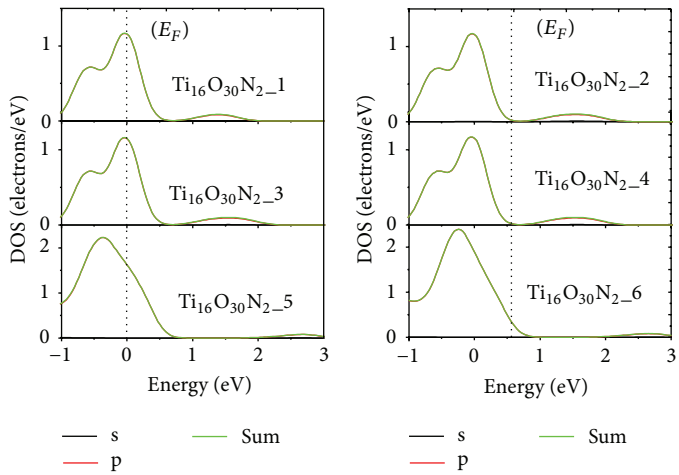

Figure 7: The density of states of neighbors bit N atom.

the super cell was (2×2×2), the NN neighbor position would have a different doping effect which has a close relationship with the distance of the two N atoms. From Figure 4 the structure optimized model also shows us the two atoms become more stable and closer to each other. So, we take Model 1 as our basis in the follow-up study of electrical neutral doping while we continue an electrical neutral study.

3.3. Comparative Analysis of Electrical Neutral Doping $Ti_{16}O_{29}N_2$ Model. Based on the partial results of the analysis, we select model 1 in Figure 4 in this section as a basic doping blueprint and then consider the case when the position of the oxygen is vacancy.

3.3.1. Eight Geometrical Structure Models of $Ti_{16}O_{29}N_2$. On the basis of the distance between an O atom and a Ti atom and their corresponding angle, we set 8 models of comparative analysis. As the selected super cell still follows in the previous section, thus the initial parameters are still without any change.

The black circle in Figure 8 is the missing oxygen atoms. Black lines represent the oxygen atoms which form a bond before they miss. We found that oxygen deletion does not cause big changes in the crystal structure. That means the geometry of the optimization is still in the acceptable range which corresponds to the actual situation, From this state, we discover that in daily growth of the crystal, oxygen atoms in rutile crystal will be easier to form such kind of vacancy, but when the oxygen has been lost, catalytic reaction may get lower effect and lower oxidation resistance. When research of impurity atoms appeared, whether it can be more effective to inhibit oxygen atoms will be the focus of it. In physics, it was easier to explain through their electronic structure.

By analyzing the results in Table 4, it is easy to see each doping crystal in the electronic structure tends to move to the valence band from Fermi level. If the impurity level gets through the Fermi level, it becomes more sensitive to light. Meanwhile, from Table 4, we know Model 7 has the lowest total energy. After analyzing the N–N distance and the angle between N–O–N atoms, we find different oxygen vacancies in different positions may cause different forms though dual N atoms are in the same position. Obviously, for Model 7 the distance between two atoms is significantly increased. Comparing the geometry of the model 7, we find the vacancy of oxygen atom is in Adjacent positions of the two N atoms. Compared to the distance of Model 1, Model 3, Model 4, Model 5, and Model 6, its deformation is relatively small, as the vacant positions are in the opposite angle between the two N atoms. Missing 2 electrons, two N atoms have to fill the vacancy position, so the two N atoms must move to fill the vacancy, which actually opened the distance between

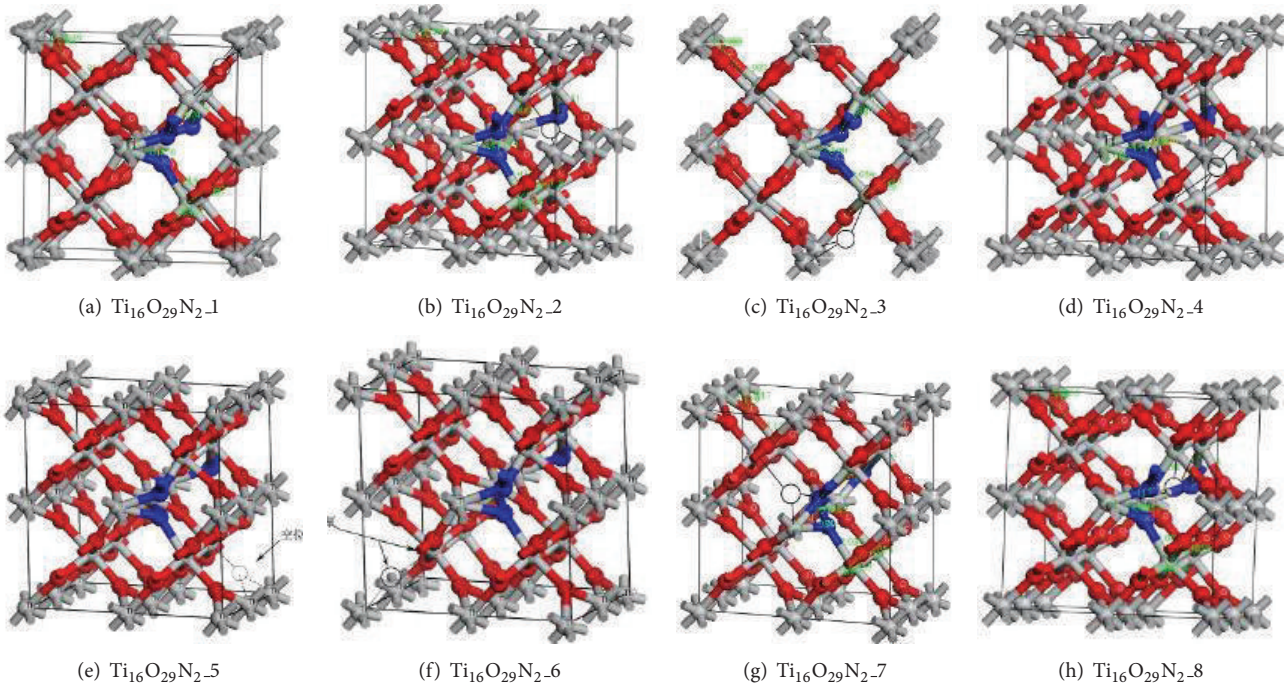

Figure 8: The structures of eight kinds of $Ti_{16}O_{29}N_2$.

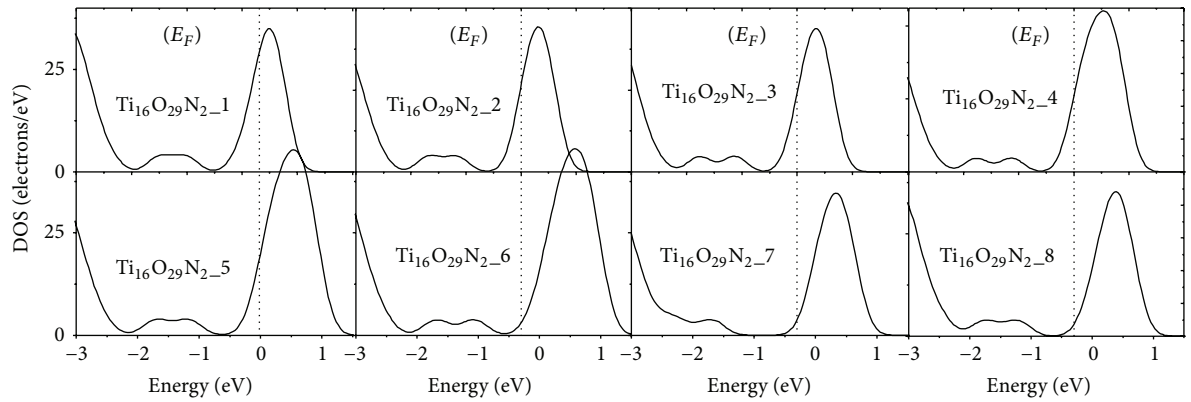

Figure 9: The total density of states of eight kinds of $Ti_{16}O_{29}N_2$ model.

two atoms which comply with the conclusion of the previous section. It has been reflected that crystals among atoms are all mutually shared electrons as they all lose necessary electrons; then it may achieve electronic balance. In this section, because of the absence of electrons, atoms around the vacant position have to coshare their electrons. Without a doubt, in actual situation, N atoms still present in the form of doped ions. Thus, the anionic dopants obtain more advantages than cation in specific tests.

3.3.2. The Electronic Structure of Eight Kinds of $Ti_{16}O_{29}N_2$ Models. In the former part, a qualitative analysis is taken from the geometry optimized structure from the figure of eight models. Then, a further analysis is taken from the perspective of the electronic structure to study the interaction among atoms which have electronic structure changes.

From Figure 9 we can see the total density of eight models is very different from the density graph where oxygen is not vacant. They have smaller band gap. For Fermi level has got into the conduction band, it indicates that the introduction of oxygen vacancy makes the eight models form a typically *n*-type semiconductor. The occupation of conduction band spread all super cells. By analyzing the occupation of conduction band, it is known that excess electrons near oxygen vacancies have made great contribution to the valence band, which have caused changes of valence band.

Figures 10 and 11 give us the N-atom and Ti atom which is in the orthoposition of the density of states. From Figure 11, we can see that N 2p's orbital is in the valence band, and its valence band level has been reduced which cannot form intermediate level. The state indicates contribution of the N atoms to light catalytic is not as good as vacant oxygen atoms.

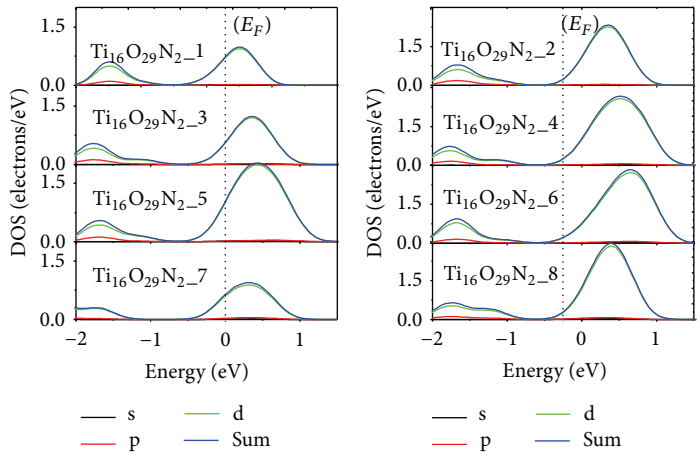

Figure 10: The DOS of Ti atom of eight kinds.

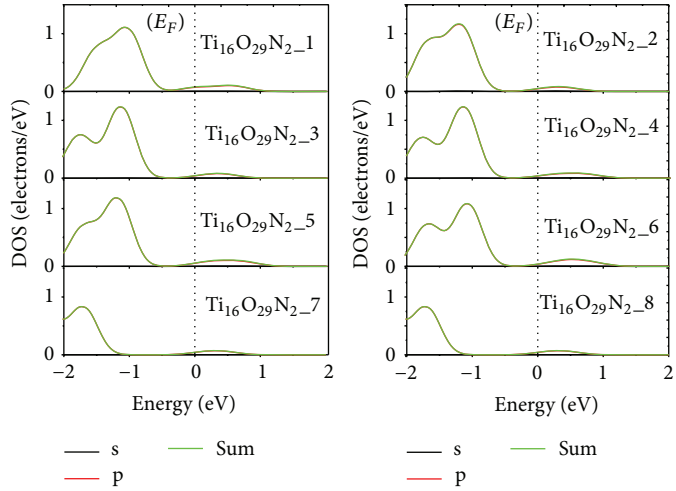

Figure 11: The DOS of N atom of eight kinds.

Figure 9 shows that the model 7, the model 8 significantly reduced the number of electrons in the valence band, and the band gap is large. The valence band and the conduction band electrons of Ti of model 7 are also reduced accordingly in Figure 10. Consider a large number of electrons need to be compensated to fill the oxygen vacancies, thus leading the conduction band moves to the Fermi level. To the whole trend, Model 7 also has some semiconductor properties, and there remains a certain band gap. However, as the impurity levels are near the Fermi energy, we cannot clearly calculate the forbidden band of the state.

4. Conclusion

In this paper, the study concludes that the growth of rutile in the natural process always rises oxygen vacancy. By theoretical calculation and analysis, we found reasons for its formation are consistent with the scientific premise.

By means of the N-doping research in the first part, it has the lower total energy, but not necessarily the smallest band gap when the dual N doped is in the nearest neighbor position. Smallest band gap appears in symmetrical position. After further research we found that the band gap becomes smaller as impurity energy level appeared in the Fermi level, while the bandwidth between conduction band and the valence band is not reduced obviously. We selected one of the models to continue the study of objects. The second part is for the selected model, where we introduce an oxygen vacancy situation to show that when the two neighboring oxygen atoms and nitrogen atoms are in its back position, the energy is the lowest and most stable. From the band structure and density analysis it is also found that the increase of the vacancy doping leads the metal atoms to move to Fermi level and then generate the N type semiconductor material. The effort of impurity elements is limited, but the catalytic activity is not as good as dual N situation. This is consistent with reality. As the rutile crystal growth usually causes daily oxygen vacancies, the oxygen vacancy has to be taken carefully, be reduced as good as we can, and then increased the doping density of ion.

Conflict of Interests

The author declares that there is no conflict of interests regarding the publication of this paper.

References

[1] A. Fujishima and K. Honda, "Electrochemical photolysis of water at a semiconductor electrode," *Nature*, vol. 238, no. 5358, pp. 37–38, 1972.

[2] R. M. Dreizler and E. K. Geoss, *Density Functional Theory*, Springer, Berlin, Germany, 1990.

[3] W. E. Pickett, "Pseudopotential methods in condensed matter applications," *Computer Physics Reports*, vol. 9, no. 3, pp. 115–197, 1989.

[4] P. Hohenberg and W. Kohn, "Inhomogeneous electron gas," *Physical Review B*, vol. 136, pp. B864–B871, 1964.

[5] R. G. Parr and W. Yang, in *Density-Functional Theory of Atoms and Molecules*, Oxford University Press, Oxford, UK, 1989.

[6] J. Zhu, F. Chen, J. Zhang, H. Chen, and M. Anpo, "Fe^{3+}-TiO_2 photocatalysts prepared by combining sol-gel method with hydrothermal treatment and their characterization," *Journal of Photochemistry and Photobiology A: Chemistry*, vol. 180, no. 1-2, pp. 196–204, 2006.

[7] S.-X. Wu, Z. Ma, Y.-N. Qin, X.-Z. Qi, and Z.-C. Liang, "Photocatalytic redox activity of doped nanocrystalline TiO_2," *Acta Physico—Chimica Sinica*, vol. 20, no. 2, pp. 138–143, 2004 (Chinese).

[8] P. Cheng, M. Y. Gu, and Y. P. Jin, "Recent progress in titania photocatalyst operating under visible light," *Progress in Chemistry*, vol. 17, no. 1, pp. 8–14, 2005.

[9] W. Zhang, Y. Li, S. Zhu, and F. Wang, "Copper doping in titanium oxide catalyst film prepared by dc reactive magnetron sputtering," *Catalysis Today*, vol. 93-95, pp. 589–594, 2004.

[10] J. T. Chang, Y. F. Lai, and J. L. He, "Photocatalytic performance of chromium or nitrogen doped arc ion plated-TiO_2 films," *Surface and Coatings Technology*, vol. 200, no. 5-6, pp. 1640–1644, 2005.

[11] U. Diebold, "The surface science of titanium dioxide," *Surface Science Reports*, vol. 48, no. 5–8, pp. 53–229, 2003.

[12] C. di Valentin, G. Pacchioni, and A. Selloni, "Theory of carbon doping of titanium dioxide," *Chemistry of Materials*, vol. 17, no. 26, pp. 6656–6665, 2005.

[13] S. Na-Phattalung, M. F. Smith, K. Kim et al., "First-principles study of native defects in anatase TiO_2," *Physical Review B*, vol. 73, no. 12, Article ID 125205, 2006.

[14] G. Mattioli, F. Filippone, P. Alippi, and A. A. Bonapasta, "*Ab initio* study of the electronic states induced by oxygen vacancies in rutile and anatase TiO_2," *Physical Review B*, vol. 78, no. 24, Article ID 241201, 2008.

[15] E. Cho, S. Han, H.-S. Ahn, K.-R. Lee, S. K. Kim, and C. S. Hwang, "First-principles study of point defects in rutile TiO_2-x," *Physical Review B: Condensed Matter and Materials Physics*, vol. 73, no. 19, Article ID 193202, 2006.

[16] M. Cococcioni and S. de Gironcoli, "Linear response approach to the calculation of the effective interaction parameters in the LDA+U method," *Physical Review B—Condensed Matter and Materials Physics*, vol. 71, no. 3, Article ID 035105, 2005.

[17] H. Iddir, S. Öğüt, P. Zapol, and N. D. Browning, "Diffusion mechanisms of native point defects in rutile TiO_2: Ab initio total-energy calculations," *Physical Review B*, vol. 75, no. 7, Article ID 073203, 2007.

[18] J. He, R. K. Behera, M. W. Finnis et al., "Prediction of high-temperature point defect formation in TiO_2 from combined *ab initio* and thermodynamic calculations," *Acta Materialia*, vol. 55, no. 13, pp. 4325–4337, 2007.

[19] E. Finazzi, C. Di Valentin, G. Pacchioni, and A. Selloni, "Excess electron states in reduced bulk anatase TiO_2: comparison of standard GGA, GGA+U, and hybrid DFT calculations," *Journal of Chemical Physics*, vol. 129, no. 15, Article ID 154113, 2008.

[20] K. Yang, Y. Dai, B. Huang, and Y. P. Feng, "Density-functional characterization of antiferromagnetism in oxygen-deficient anatase and rutile TiO_2," *Physical Review B: Condensed Matter and Materials Physics*, vol. 81, no. 3, Article ID 033202, 2010.

[21] Z. Lin, A. Orlov, R. M. Lambert, and M. C. Payne, "New insights into the origin of visible light photocatalytic activity of nitrogen-doped and oxygen-deficient anatase TiO_2," *Journal of Physical Chemistry B*, vol. 109, no. 44, pp. 20948–20952, 2005.

[22] Y. Nakano, T. Morikawa, T. Ohwaki, and Y. Taga, "Deep-level optical spectroscopy investigation of N-doped TiO_2 films," *Applied Physics Letters*, vol. 86, no. 13, Article ID 132104, pp. 1–3, 2005.

[23] C. Di Valentin, G. Pacchioni, and A. Selloni, "Origin of the different photoactivity of N-doped anatase and rutile TiO_2," *Physical Review B: Condensed Matter and Materials Physics*, vol. 70, no. 8, Article ID 85116, 2004.

[24] H. Noda, K. Oikawa, T. Ogata, K. Matsuki, and H. Kamata, "Preparation of titanium (IV) oxides and its characterization," *Journal of the Chemical Society of Japan*, no. 8, pp. 1084–1090, 1986 (Japanese).

[25] I. Justicia, P. Ordej, G. Canto et al., "Designed self-doped titanium oxide thin films for efficient visible-light photocatalysis," *Advanced Materials*, vol. 14, p. 1399, 2002.

[26] I. Nakamura, N. Negishi, S. Kutsuna, T. Ihara, S. Sugihara, and K. Takeuchi, "Role of oxygen vacancy in the plasma-treated TiO_2 photocatalyst with visible light activity for NO removal," *Journal of Molecular Catalysis A: Chemical*, vol. 161, no. 1-2, pp. 205–212, 2000.

[27] T. Ihara, M. Miyoshi, Y. Iriyama, O. Matsumoto, and S. Sugihara, "Visible-light-active titanium oxide photocatalyst realized by an oxygen-deficient structure and by nitrogen doping," *Applied Catalysis B: Environmental*, vol. 42, no. 4, pp. 403–409, 2003.

[28] T. Ihara, M. Ando, and S. Sugihara, "Preparation of visible light active TiO_2 photocatalysis using wet method," *Photocatalysis*, vol. 5, p. 19, 2001.

[29] A. K. Rumaiz, J. C. Woicik, E. Cockayne, H. Y. Lin, G. H. Jaffari, and S. I. Shah, "Oxygen vacancies in N doped anatase TiO_2: experiment and first-principles calculations," *Applied Physics Letters*, vol. 95, no. 26, Article ID 262111, 2009.

[30] H. Irie, Y. Watanabe, and K. Hashimoto, "Nitrogen-concentration dependence on photocatalytic activity of $TiO_{2-x}N_x$ powders," *The Journal of Physical Chemistry B*, vol. 107, no. 23, pp. 5483–5486, 2003.

[31] J. Wang, D. N. Tafen, J. P. Lewis et al., "Origin of photocatalytic activity of Nitrogen-doped TiO_2 nanobelts," *Journal of the American Chemical Society*, vol. 131, no. 34, pp. 12290–12297, 2009.

[32] E. Obuchi, "Titania photocatalytic," *Journal of the Electrochemical Society*, vol. 143, no. 9, pp. 191–193, 1996.

[33] A. L. Linsebigler, G. Lu, and J. T. Yates Jr., "Photocatalysis on TiO_2 surfaces: principles, mechanisms, and selected results," *Chemical Reviews*, vol. 95, no. 3, pp. 735–758, 1995.

[34] M. Wu, W. Zhang, Z. Du, and Y. Huang, "Structural transformation in nanophase titanium dioxide," *Modern Physics Letters B*, vol. 13, no. 5, pp. 167–174, 1999.

[35] T. Ohno, K. Tokieda, S. Higashida, and M. Matsumura, "Synergism between rutile and anatase TiO_2 particles in photocatalytic oxidation of naphthalene," *Applied Catalysis A: General*, vol. 244, no. 2, pp. 383–391, 2003.

[36] G. Zheng, S. J. Clark, P. R. Tulip, S. Brand, and R. A. Abram, "Ab initio dynamics study of poly-para-phenylene vinylene," *Journal of Chemical Physics*, vol. 123, no. 2, Article ID 024904, 2005.

[37] G. Zheng, S. J. Clark, S. Brand, and R. A. Abram, "First-principles studies of the structural and electronic properties of poly-*para*-phenylene vinylene," *Journal of Physics Condensed Matter*, vol. 16, no. 47, pp. 8609–8620, 2004.

[38] G. Zheng, S. J. Clark, S. Brand, and R. A. Abram, "Lattics dynamics of polymer PPyV and PANI: first-principles determination," *Physical Review B*, vol. 74, Article ID 165210, 2006.

[39] K. H. He, G. Zheng, G. Chen, T. Lü, M. Wan, and G. F. Ji, "Effects of single oxygen vacancy on electronic structure and ferromagnetism for V-doped TiO_2," *Solid State Communications*, vol. 144, no. 1-2, pp. 54–57, 2007.

[40] W. Xue D, J. Cai, M. Wang X et al., "First-principle study on $SrTiO_3$ film oxygen imperfection," *Journal of Atomic and Molecular Physics*, vol. 24, no. 4, pp. 875–878, 2007.

[41] Q. Feng, X. Q. Wang, and G. B. Liu, "First-principles study of point defects in rutile TiO_2," *Journal of Physics B: Atomic and Molecular Physics*, vol. 25, no. 5, article 1096, 2008 (Chinese).

[42] Y. G. Liu, M. X. Song, L. Bian, T. Zhou, and X. Zhao, "Ab initio band gap calculation of rare earth doped rutile TiO_2," *Journal of Atomic and Molecular Physics*, vol. 25, no. 5, p. 1141, 2008 (Chinese).

[43] J. P. Perdew, K. Burke, and M. Ernzerhof, "Generalized gradient approximation made simple," *Physical Review Letters*, vol. 77, no. 18, pp. 3865–3868, 1996.

[44] M. D. Segall, P. J. D. Lindan, M. J. Probert et al., "First-principles simulation: ideas, illustrations and the CASTEP code," *Journal of Physics Condensed Matter*, vol. 14, no. 11, pp. 2717–2744, 2002.

[45] Q. T. Song, P. Yang, J. B. Wang, X. Lu, and N. Huang, "First-principles study on the rutile TiO_2 doped with phosphorus," *Journal of Materials Science & Engineering*, vol. 26, no. 3, pp. 435–437, 2008.

[46] Q. L. Chen and C. Q. Tang, "Ab initio band calculations of transition metals doped rutile TiO_2," *Journal of Materials Science & Engineering*, vol. 24, no. 4, p. 514, 2006.

[47] J. G. Traylor, H. G. Smith, R. M. Nicklow, and M. K. Wilkinson, "Lattice dynamics of rutile," *Physical Review B*, vol. 3, no. 10, pp. 3457–3472, 1971.